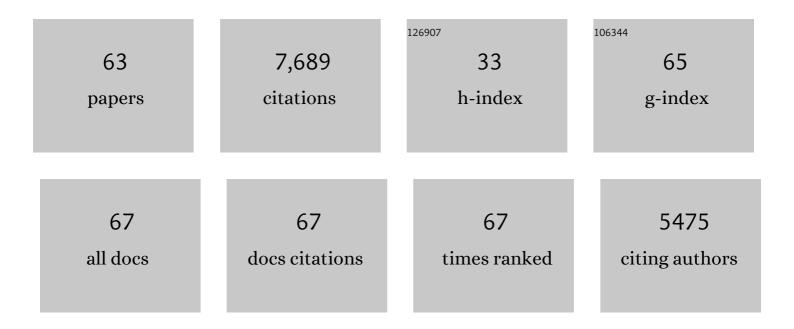
List of Publications by Year in descending order

Source: https://exaly.com/author-pdf/3381827/publications.pdf Version: 2024-02-01



KUDT L FEICI

#	Article	IF	CITATIONS
1	Radar interferometry and its application to changes in the Earth's surface. Reviews of Geophysics, 1998, 36, 441-500.	23.0	1,992
2	The displacement field of the Landers earthquake mapped by radar interferometry. Nature, 1993, 364, 138-142.	27.8	1,853
3	Intrusion triggering of the 2010 Eyjafjallajökull explosive eruption. Nature, 2010, 468, 426-430.	27.8	366
4	Coseismic and Postseismic Fault Slip for the 17 August 1999, M = 7.5, Izmit, Turkey Earthquake. Science, 2000, 289, 1519-1524.	12.6	273
5	Radar interferometric mapping of deformation in the year after the Landers earthquake. Nature, 1994, 369, 227-230.	27.8	267
6	Space geodetic measurement of crustal deformation in central and southern California, 1984–1992. Journal of Geophysical Research, 1993, 98, 21677-21712.	3.3	247
7	Discrimination of geophysical phenomena in satellite radar interferograms. Geophysical Research Letters, 1995, 22, 1537-1540.	4.0	208
8	Surface motion of mountain glaciers derived from satellite optical imagery. Remote Sensing of Environment, 2005, 95, 14-28.	11.0	195
9	Crustal deformation and fault slip during the seismic cycle in the North Chile subduction zone, from GPS and InSAR observations. Geophysical Journal International, 2004, 158, 695-711.	2.4	139
10	Fault slip distribution of two June 2000 M W 6.5 earthquakes in South Iceland estimated from joint inversion of InSAR and GPS measurements. Earth and Planetary Science Letters, 2003, 213, 487-502.	4.4	123
11	Active tectonics of the western Mediterranean: Geodetic evidence for rollback of a delaminated subcontinental lithospheric slab beneath the Rif Mountains, Morocco. Geology, 2006, 34, 529.	4.4	122
12	Ground motion response to an ML 4.3 earthquake using co-located distributed acoustic sensing and seismometer arrays. Geophysical Journal International, 2018, 213, 2020-2036.	2.4	122
13	Geodetic measurement of tectonic deformation in the Santa Maria Fold and Thrust Belt, California. Journal of Geophysical Research, 1990, 95, 2679-2699.	3.3	93
14	Crustal deformation near Hengill volcano, Iceland 1993-1998: Coupling between magmatic activity and faulting inferred from elastic modeling of satellite radar interferograms. Journal of Geophysical Research, 2000, 105, 25655-25670.	3.3	93
15	RNGCHN: a program to calculate displacement components from dislocations in an elastic half-space with applications for modeling geodetic measurements of crustal deformation. Computers and Geosciences, 1999, 25, 695-704.	4.2	84
16	Estimating Slip Distribution for the Izmit Mainshock from Coseismic GPS, ERS-1, RADARSAT, and SPOT Measurements. Bulletin of the Seismological Society of America, 2002, 92, 138-160.	2.3	80
17	Magma injection into a longâ€lived reservoir to explain geodetically measured uplift: Application to the 2007–2014 unrest episode at Laguna del Maule volcanic field, Chile. Journal of Geophysical Research: Solid Earth, 2016, 121, 6092-6108.	3.4	73
18	Estimation of an earthquake focal mechanism from a satellite radar interferogram: Application to the December 4, 1992 Landers aftershock. Geophysical Research Letters, 1995, 22, 1037-1040.	4.0	66

#	Article	IF	CITATIONS
19	Rapid uplift in Laguna del Maule volcanic field of the Andean Southern Volcanic zone (Chile) 2007–2012. Geophysical Journal International, 2014, 196, 885-901.	2.4	65
20	Dynamics of a large, restless, rhyolitic magma system at Laguna del Maule, southern Andes, Chile. CSA Today, 2014, , 4-10.	2.0	63
21	Satellite radar interferometric map of the coseismic deformation field of the M = 6.1 Eureka Valley, California Earthquake of May 17, 1993. Geophysical Research Letters, 1995, 22, 1541-1544.	4.0	57
22	Evolution of unrest at Laguna del Maule volcanic field (Chile) from InSAR and GPS measurements, 2003 to 2014. Geophysical Research Letters, 2015, 42, 6590-6598.	4.0	57
23	Kinematic models of plate boundary deformation in southwest Iceland derived from GPS observations. Journal of Geophysical Research, 2006, 111, .	3.3	55
24	Analysis of coseismic surface displacement gradients using radar interferometry: New insights into the Landers earthquake. Journal of Geophysical Research, 1994, 99, 21971-21981.	3.3	54
25	Coseismic deformation field of the M=6.7 Northridge, California Earthquake of January 17, 1994 recorded by two radar satellites using interferometry. Geophysical Research Letters, 1996, 23, 969-972.	4.0	47
26	A method for modelling radar interferograms without phase unwrapping: application to the M 5 Fawnskin, California earthquake of 1992 December 4. Geophysical Journal International, 2009, 176, 491-504.	2.4	46
27	Triggered fault slip on June 17, 2000 on the Reykjanes Peninsula, SW-Iceland captured by radar interferometry. Geophysical Research Letters, 2003, 30, .	4.0	44
28	Twenty-five years of geodetic measurements along the Tadjoura-Asal rift system, Djibouti, East Africa. Journal of Geophysical Research, 2007, 112, .	3.3	43
29	Mouvements actuels des blocs tectoniques dans l'arc Bético-Rifain à partir des mesures GPS entre 1999 et 2005. Comptes Rendus - Geoscience, 2008, 340, 400-413.	1.2	43
30	Nonlinear estimation of geometric parameters in FEMs of volcano deformation: Integrating tomography models and geodetic data for Okmok volcano, Alaska. Journal of Geophysical Research, 2012, 117, .	3.3	41
31	Geomorphic expression of rapid Holocene silicic magma reservoir growth beneath Laguna del Maule, Chile. Science Advances, 2018, 4, eaat1513.	10.3	38
32	Postseismic deformation following the June 2000 earthquake sequence in the south Iceland seismic zone. Journal of Geophysical Research, 2005, 110, .	3.3	36
33	The Al Hoceima (Morocco) earthquake of 24 February 2004, analysis and interpretation of data from ENVISAT ASAR and SPOT5 validated by ground-based observations. Remote Sensing of Environment, 2009, 113, 306-316.	11.0	35
34	Geodetic measurement of tectonic deformation in the southern Alps and Provence, France, 1947–1994. Earth and Planetary Science Letters, 1998, 159, 35-46.	4.4	32
35	Coseismic interferograms of two MS=6.6 earthquakes in the South Iceland Seismic Zone, June 2000. Geophysical Research Letters, 2001, 28, 3341-3344.	4.0	31
36	Surface effects of faulting and deformation resulting from magma accumulation at the Hengill triple junction, SW Iceland, 1994–1998. Journal of Volcanology and Geothermal Research, 2002, 115, 233-255.	2.1	31

#	Article	IF	CITATIONS
37	Geodetic observations of post-seismic transients in the context of the earthquake deformation cycle. Comptes Rendus - Geoscience, 2006, 338, 1012-1028.	1.2	31
38	Crustal deformation associated with the 1996 Gjálp subglacial eruption, Iceland: InSAR studies in affected areas adjacent to the Vatnajökull ice cap. Earth and Planetary Science Letters, 2007, 259, 24-33.	4.4	30
39	Applying differential InSAR to orbital dynamics: a new approach for estimating ERS trajectories. Journal of Geodesy, 2003, 77, 493-502.	3.6	29
40	InSAR observations and models of crustal deformation due to a glacial surge in Iceland. Geophysical Journal International, 2014, 198, 1329-1341.	2.4	28
41	Geodetic measurement of horizontal strain across the Red River fault near Thac Ba, Vietnam, 1963-1994. Journal of Geodesy, 1999, 73, 298-310.	3.6	27
42	Volcano deformation source parameters estimated from InSAR: Sensitivities to uncertainties in seismic tomography. Journal of Geophysical Research: Solid Earth, 2016, 121, 3002-3016.	3.4	27
43	Geothermal production and reduced seismicity: Correlation and proposed mechanism. Earth and Planetary Science Letters, 2018, 482, 470-477.	4.4	22
44	Geodetic measurements and numerical models of rifting in Northern Iceland for 1993–2008. Geophysical Journal International, 2014, 196, 1267-1280.	2.4	20
45	Geothermal reservoir characterization using distributed temperature sensing at Brady Geothermal Field, Nevada. The Leading Edge, 2017, 36, 1024a1-1024a7.	0.7	20
46	Aftershock Distribution as a Constraint on the Geodetic Model of Coseismic Slip for the 2004 Parkfield Earthquake. Pure and Applied Geophysics, 2011, 168, 1553-1565.	1.9	19
47	37 Estimating earthquake source parameters from geodetic measurements. International Geophysics, 2002, , 607-XIV.	0.6	18
48	Deformation studies at Furnas and Sete Cidades Volcanoes (São Miguel Island, Azores). Velocities and further investigations. Geophysical Journal International, 2006, 166, 952-956.	2.4	18
49	Optimizing geothermal production in fractured rock reservoirs under uncertainty. Geothermics, 2020, 88, 101906.	3.4	18
50	A scheme for reducing the effect of selective availability on precise geodetic measurements from the Global Positioning System. Geophysical Research Letters, 1991, 18, 1289-1292.	4.0	16
51	First epoch geodetic GPS measurements across the Afar Plate Boundary Zone. Geophysical Research Letters, 1993, 20, 1899-1902.	4.0	16
52	Ground deformation in an area later damaged by an earthquake: monitoring the Avcilar district of Istanbul, Turkey, by satellite radar interferometry 1992-1999. Geophysical Journal International, 2009, 178, 976-988.	2.4	15
53	Graph theory for analyzing pair-wise data: application to geophysical model parameters estimated from interferometric synthetic aperture radar data at Okmok volcano, Alaska. Journal of Geodesy, 2017, 91, 9-24.	3.6	15
54	Three-dimensional mechanical models for the June 2000 earthquake sequence in the south Iceland seismic zone. Tectonophysics, 2008, 457, 12-29.	2.2	13

#	Article	IF	CITATIONS
55	Inferring Geothermal Reservoir Processes at the Raft River Geothermal Field, Idaho, USA, Through Modeling <scp>InSAR</scp> â€Measured Surface Deformation. Journal of Geophysical Research: Solid Earth, 2018, 123, 3645-3666.	3.4	13
56	The level of the GrÃmsvötn subglacial lake, Vatnajökull, Iceland, monitored with SPOT5 images. Earth and Planetary Science Letters, 2006, 243, 293-302.	4.4	12
57	A new strategy for estimating geophysical parameters from InSAR data: Application to the Krafla central volcano in Iceland. Geochemistry, Geophysics, Geosystems, 2012, 13, .	2.5	11
58	InSAR time series analysis of the 9 July 1998 Azores earthquake. International Journal of Remote Sensing, 2005, 26, 2715-2729.	2.9	10
59	Characterizing volumetric strain at Brady Hot Springs, Nevada, USA using geodetic data, numerical models and prior information. Geophysical Journal International, 2018, 215, 1501-1513.	2.4	7
60	Geodetic Measurements and Numerical Models of Deformation at Coso Geothermal Field, California, USA, 2004–2016. Remote Sensing, 2020, 12, 225.	4.0	6
61	Geodetic measurements and numerical models of transient deformation at Raft River geothermal field, Idaho, USA. Geothermics, 2018, 74, 106-111.	3.4	5
62	Timeâ€5eries Analysis of Volume Change at Brady Hot Springs, Nevada, USA, Using Geodetic Data From 2003–2018. Journal of Geophysical Research: Solid Earth, 2020, 125, e2019JB017816.	3.4	4
63	Spatio–Temporal Analysis of Deformation at San Emidio Geothermal Field, Nevada, USA Between 1992 and 2010. Remote Sensing, 2019, 11, 1935.	4.0	1